Targeted molecular imaging in oncology

David J. Yang,* E. Edmund Kim* and Tomio Inoue**

*Department of Experimental Diagnostic Imaging, The University of Texas M.D. Anderson Cancer Center, Houston, TX, USA
**Department of Radiology, Yokohama City University, Yokohama, Japan

Improvement of scintigraphic tumor imaging is extensively determined by the development of more tumor specific radiopharmaceuticals. Thus, to improve the differential diagnosis, prognosis, planning and monitoring of cancer treatment, several functional pharmaceuticals have been developed. Application of molecular targets for cancer imaging, therapy and prevention using generator-produced isotopes is the major focus of ongoing research projects. Radionuclide imaging modalities (positron emission tomography, PET; single photon emission computed tomography, SPECT) are diagnostic cross-sectional imaging techniques that map the location and concentration of radionuclide-labeled radiotracers. ^{99m}Tc- and ^{68}Ga-labeled agents using ethylenedicysteine (EC) as a chelator were synthesized and their potential uses to assess tumor targets were evaluated. ^{99m}Tc ($t_{1/2}$ = 6 hr, 140 keV) is used for SPECT and ^{68}Ga ($t_{1/2}$ = 68 min, 511 keV) for PET. Molecular targets labeled with Tc-99m and Ga-68 can be utilized for prediction of therapeutic response, monitoring tumor response to treatment and differential diagnosis. Molecular targets for oncological research in (1) cell apoptosis, (2) gene and nucleic acid-based approach, (3) angiogenesis (4) tumor hypoxia, and (5) metabolic imaging are discussed. Numerous imaging ligands in these categories have been developed and evaluated in animals and humans. Molecular targets were imaged and their potential to redirect optimal cancer diagnosis and therapeutics were demonstrated.

Key words: ethylenedicysteine, cancer, imaging, technetium-99m, gallium-68

INTRODUCTION

ASSESSMENT OF THE EFFECTIVENESS of cancer therapy (e.g. volumetric and morphological changes) is measured by CT and MRI. In addition to these imaging modalities, the treatment endpoints rely almost exclusively on the analysis of biopsies by molecular and histopathological methods. These methods provide a microscopic picture of the general heterogeneous process. Therefore, to assess clinical endpoints adequately, a specific target assessment marker is needed that would allow precise measurement of tumor targets on a whole-body image upon administration of a functional agent. These mechanism-based agents provide image-guided therapy which may allow discontinuation of ineffective treatment in an earlier phase and switch to a more efficient treatment that would be beneficial to patients early on in the course of treatment.

PET and SPECT use radiotracers to image, map and measure target site activities (e.g. angiogenesis, metabolism, apoptosis and proliferation) and they are considered as molecular imaging modalities.[1–3] Reliable molecular imaging assays that assess (1) cellular targets at low cost (2) treatment response more rapidly, (3) differential diagnosis, (4) the prediction of therapeutic response, and (5) better radiation dosimetry for internal radiotherapy would be very valuable. Here, we report a series of tumor-specific agents that may provide potential applications in differential diagnosis and prediction of early treatment response.

Selection of isotopes and chemistry chelators for imaging

To develop novel or clinically used tracers, two types of chemistries are frequently used in the preparation of radiotracers: covalent and ionic. In covalent chemistry, either displacement or addition reactions are used to place an isotope in the molecule. The labeled product provides minimal structural alteration; however, the procedure may be lengthy, tedious, with low yield, and costly. Isotopes commonly used in covalent chemistry include ^{18}F, ^{123}I, ^{131}I, ^{75}Br, ^{77}Br and ^{11}C. In complex chemistry, a chelator is required to trap metal isotopes. This type of chemistry is simple and with high yield. The isotopes may be obtained from generators. Though complex chemistry is attractive, the chemical properties may be altered due to the addition of a chelator.

Among all SPECT radioisotopes, ^{99m}Tc has been preferred to label radiopharmaceuticals due to favorable low energy (140 keV), inexpensive isotope cost ($0.21/mCi) and easy chemistry. Several ^{99m}Tc-labeling chelators have been reported such as N_4 (e.g. Cyclam-14, DOTA), N_3S (e.g. MAG-3), N_2S_2 (e.g. ECD), NS_3, S_4 (e.g. sulfur colloid), diethylenetriamine pentaacetic acid (DTPA), O_2S_2 (e.g. DMSA), and hydrazinenicotinamide (HYNIC).[4–10] Among these chelators, DTPA forms less stable complexes with ^{99m}Tc. ^{99m}Tc-HYNIC has been shown to be useful in imaging, but labeling HYNIC with ^{99m}Tc requires two chemicals, thiphenylphosphine and tricine, which are inconvenient for the kit preparation. The nitrogen and sulfur combination has been shown to be a stable chelator for ^{99m}Tc-bis-aminoethanethiol tetradentate ligands, also called diaminodithiol compounds, which are known to form very stable Tc(V)O-complexes on the basis of efficient binding of the oxotechnetium group to two thiosulfur and two amine nitrogen atoms. L,L-Ethylenedicysteine (EC) is the most successful example of N_2S_2 chelates.[6] EC can be labeled with both ^{68}Ga and ^{99m}Tc efficiently with high radiochemical purity and the preparation remains stable for several hours.[11–21]

In addition to assessing molecular targets, ^{99m}Tc might be useful in planning internal targeted radionuclide therapy with ^{188}Re-labeled agents. ^{188}Re has good characteristics for imaging and for potential therapeutic use because of its high β energy (2.1 MeV), short physical half-life (16.9 hr) and 155 keV γ-ray emission for dosimetric and imaging purposes. The short physical half-life of ^{188}Re allows for higher doses compared with long-lived radionuclides. Furthermore, the short half-life reduces the problems of radioactive waste handing and storage. In particular, ^{188}Re is available from an in-house generator system similar to a ^{99m}Tc generator. ^{188}Re can be obtained from a ^{188}W/^{188}Re generator, which makes it very convenient for clinical use. Both ^{99m}Tc and ^{188}Re emit gamma rays, so the dosimetry generated based on ^{99m}Tc images is expected to be more accurate than that produced using the current standard radioisotope, Y-90.

PET radiosynthesis must be rapid because the radioisotope will decay during lengthy chemical synthesis, and a higher risk of radiation exposure may occur during radiosynthesis. Cyclotron-based tracers are constrained by the availability of a local cyclotron and its high cost. The Food and Drug Administration (FDA) permits radiopharmaceutical production in central commercial facilities under well-controlled conditions and distribution to local clinics where they are administered. Similarly, radionuclide generator systems that can be produced in a well-controlled facility are embraced by current FDA procedures and have a long history of successful clinical application. A generator uses a parent-daughter nuclide pair wherein a relatively long-lived parent isotope decays to a short-lived daughter isotope that is used for imaging. The parent isotope, which is produced at a cyclotron facility, can be shipped to a clinical site from which the daughter isotope may be eluted on site for clinical use. In our case, ^{68}Ga-based PET agents possess significant commercial potential because the isotope can be produced from a ^{68}Ge generator (275-day half-life) on site and serve as a convenient alternative to cyclotron-based PET isotopes, such as ^{18}F or ^{124}I.

^{68}Ga has a high positron emitting quantity (89% of its total decay), and therefore the main consideration is its spatial resolution, which depends on the positron range (energy), the non-colinearity of annihilating photons, intrinsic properties, size and geometry of the detector and the selection of the reconstruction algorithm. Aspects of the detector design, physical properties and their influence on system spatial resolution have been extensively addressed by many authors, leading to a continuous optimization of hardware. Although the maximum positron energy of ^{68}Ga (max = 1.90 MeV, mean = 0.89 MeV) is higher than that of ^{18}F (max = 0.63 MeV, mean = 0.25 MeV), a study using Monte Carlo analysis on spatial resolution revealed that under the assumption of 3 mm spatial resolution of PET detectors, the conventional full width at half maximum (FWHM) of ^{18}F and ^{68}Ga are indistinguishable in soft tissue (3.01 mm vs. 3.09 mm).[22,23] This implies that with the spatial resolution at 5 to 7 mm of current clinical scanners, the imaging quality using ^{68}Ga-based tracers can be as good as that of ^{18}F-based agents and has stimulated others to investigate potential ^{68}Ga-based imaging agents.[24–26]

Focus in targeted molecular imaging

Molecular imaging provides angiogenesis, cellular translational and transcriptional information. The important applications in molecular imaging in oncology are differentiation (i.e. inflammation vs. recurrence, sensitive vs. resistant) and prediction (i.e. selection of patients who are more likely to respond to therapy). The agents that could differentiate inflammation vs. tumors are apoptotic and DNA markers since they accumulate in cell nuclei. The agents that could provide therapeutic prediction are

enzymatic (hypoxia, Akt, tyrosinases) and receptor (estrogen, androgen, TRAIL) markers. In this report, a series of EC-agents and cyclam-agents in oncology target assessment are reviewed.

Assessment of apoptosis

The importance of apoptosis in determining chemotherapy response remains unclear. Some authors have suggested that apoptosis may be the most critical determinant of a tumor's sensitivity or resistance to chemotherapy.[27] However, investigations that have studied the importance of apoptosis in human solid tumors have been sparse. Studies of cervical cancer have found the baseline apoptotic index (AI) of the malignant cells to be prognostic of the clinical response to chemotherapy and overall survival.[28,29] In addition, the response of cervical cancer to cisplatin has been found to correlate with the level of therapy-induced apoptosis.[28] The importance of the baseline AI in breast cancer has never been investigated, and determining the importance of therapy-induced apoptosis in solid tumors currently remains a relatively unexplored area of clinical research.

One possible reason that there is little information concerning therapy-induced apoptosis in human tumors is that the histological evidence of apoptosis occurs within a brief period immediately after treatment. *In vivo* work has revealed that apoptosis of breast cancer cells rapidly increases to a peak after chemotherapy, and then rapidly declines to baseline levels.[30–33] In the murine mammary carcinoma, the time of greatest therapy-induced apoptosis was 24–40 hours after initiation of chemotherapy. Whether this is the optimal time in human breast cancer patients is currently unknown. Buchholz et al.[34] investigated whether changes in tumor cell apoptosis and Bcl-2 expression immediately after chemotherapy correlated with response to breast cancer treatment. Apoptosis levels were quantified by use of a fluorescent terminal deoxynucleotidyl transferase-mediated deoxyuridine triphosphate nick end-labeling (TUNEL) stain, and Bcl-2 and Bax were measured by semi-quantitative immunohistochemical assays. The apoptosis level at 48 hours was significantly higher in the tumors with pathologically complete response or < 1 cm of residual disease (median, 22%; range, 6%–51%) than in the tumors with > 1 cm residual disease (median, 7%; range, 1%–36%). A decrease in Bcl-2 expression after chemotherapy relative to the expression from the pretreatment sample also correlated with disease response. Furthermore, Symmans et al.[35] demonstrated that AI was an accurate method to detect paclitaxel-induced apoptosis in women with primary breast cancer (PBC) receiving induction chemotherapy (IC). The initial grade of the apoptotic response inversely related with the amount of residual disease at surgery. These data suggested that apoptosis may play an important role in determining breast cancer response to chemotherapy and that the level of treatment-induced apoptosis may have some value

as a predictive marker. Recently, an enzyme linked immunosorbent assay (ELISA) has been developed to detect the caspase cleavage fragment of CK18 (M30-antigen).[36] High M30-antigen levels have been demonstrated in patients with metastatic breast cancer compared to healthy controls.

We have formulated ^{99m}Tc-EC-annexin V for assessment of apoptosis in animal models.[12] When compared to ^{99m}Tc-HYNIC-annexin V in rat models, the kidneys had the highest concentration of radioactivity (% injected dose/gram) at 10 min–180 min after intravenous injection of ^{99m}Tc-HYNIC-annexin V (9.5–17) and ^{99m}Tc-EC-annexin V (4.9–6.9). ^{99m}Tc-HYNIC-annexin V had faster blood clearance than ^{99m}Tc-EC-annexin V ($t_{1/2}$ = 15 min vs. 100 min). Both agents showed similar uptake in liver and spleen and poor brain uptake.[4] Pharmacokinetic studies were conducted using ^{99m}Tc-EC-annexin V in 10 breast cancer patients. The protocol was approved by the University of Texas M.D. Anderson Cancer Center Institutional Review Board (ID-02-732). Between December 2003 and February 2004, ten patients with untreated PBC (stage II–III) were enrolled in this prospective study. After providing signed informed consent, they received a single intravenous injection of 25–29 mCi of ^{99m}Tc-EC-annexin V. Subsequently, whole body planar images using a dual-headed gamma camera were obtained at 0.5, 2–4, 18–24 hours after injection. SPECT images of the chest were also obtained 3 hours after injection. Computer outlined regions of interest (ROI) (counts per pixel) were used to determine tumor-to-background count density ratios (T/N). The ratios were used to compare dynamic tumor uptake pre- and post-treatment. Errors in the use of image ROIs as standards to correspond to anatomically relevant features have been described and found tolerable. Five of these patients received a dose of induction therapy 16 hours before the last imaging session. The induction therapy consisted of chemotherapy (paclitaxel, 2 patients; fluorouracil, doxorubicin, cyclophosphamide, FAC, 1 patient) and bcl-2 antisense oligonucleotide (Genasense™, 2 patients). In all cases, there was detectable ^{99m}Tc-EC-annexin V uptake that corresponded to the area of palpable invasive disease. The selected whole body image is shown in Figure 1. The median baseline T/N was 2.11 (range 1.32–3.30). In those patients receiving IC, the mean T/N ratio was 2.57 (range 2.05–3.30, n = 5) which was higher than in those patients without IC (mean 1.53, range 1.35–1.73, n = 4). A high T/N tended to show a better response. Based upon quantification of the serial whole body images from the clinical studies to generate estimated residence times, dosimetry of ^{99m}Tc-EC-annexin V was estimated using MIRDose 3.1. Similar to our animal studies, whole body, blood-forming organ and gonad absorbed dose estimates for the proposed single dosage of 25–29 mCi were less than the limits of 3 rem annual and 5 rem total, and those to other organs less than the limits of 5 rem annual and 15 rem total (Table 1). The
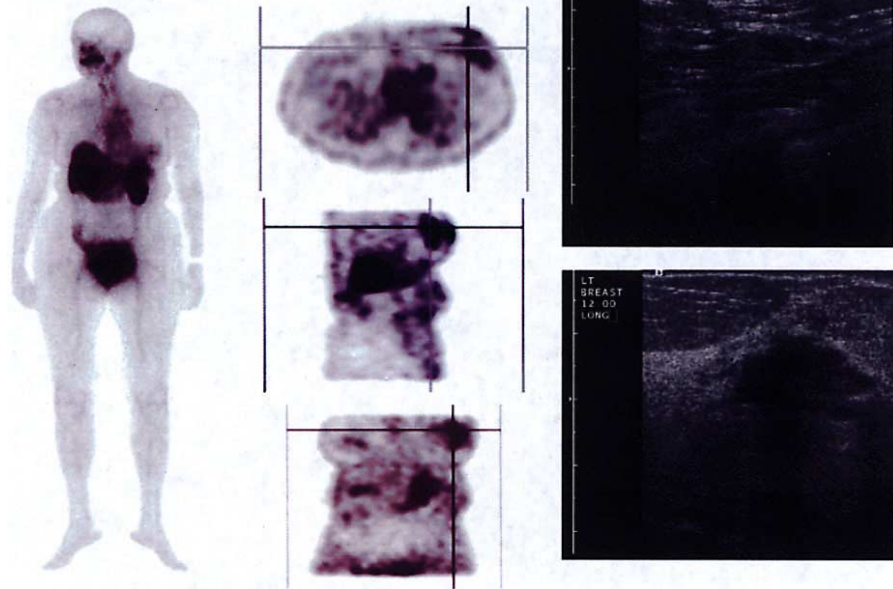
Fig. 1 A coronal whole body image (*left*) of a patient who received ^{99m}Tc-EC-annexin V (25 mCi, i.v., 3 hours) showed that the tumor in the left breast could be well visualized.

Table 1 Radiation dose estimates from human (n = 10) for the reference adult using ^{99m}Tc-EC-annexin V

Target Organ	Average rad/mCi
Adrenals	2.16E-02
Brain	1.03E-02
Breasts	9.97E-03
Gallbladder Wall	2.21E-02
LLI Wall	1.78E-02
Small Intestine	1.68E-02
Stomach	1.66E-02
ULI Wall	1.76E-02
Heart Wall	1.72E-02
Kidneys	7.40E-02
Liver	3.46E-02
Lungs	2.81E-02
Muscle	1.28E-02
Ovaries	1.82E-02
Pancreas	2.13E-02
Red Marrow	1.37E-02
Bone Surfaces	2.31E-02
Skin	8.23E-03
Spleen	3.43E-02
Thymus	1.37E-02
Thyroid	1.32E-02
Urin Bladder Wall	8.32E-02
Uterus	2.11E-02
Total Body	1.45E-02
EFF DOSE EQUIV (rem/mCi)	2.72E-02
EFF DOSE (rem/mCi)	2.33E-02

magnitude of the radiation-absorbed doses was less than those predicted based on animal doses.[12] These early data suggest that assessment of apoptosis by ^{99m}Tc-EC-annexin V could be useful to evaluate the baseline level of apoptosis, predict the efficacy of therapy based on the detection of treatment-related apoptosis and possibly predict disease progression and prognosis. Furthermore, it appears to correlate with biological markers of proliferation, suggesting a correlation with the occurrence of spontaneous apoptosis.

Assessment of gene and nucleic acid-based targets
Assessment of tumor cell proliferation by PET and SPECT could be helpful in the evaluation of tumor growth potential, the degree of malignancy and could provide an early assessment of treatment response. Several efforts have been made to assess tumor proliferative activity. It has been reported that 2′-fluorodeoxyglucose ([^{18}F]FDG) uptake is an indicator of tumor proliferative activity.[37] Higashi et al. have shown that [^{18}F]FDG uptake is strongly related to the number of viable cells.[38] Another approach was to use a radiolabeled amino acid as a tumor cell proliferative marker.[39,40] However, the structures of these agents are not purine or pyrimidine-based, which are essential building blocks of DNA. Although several radiolabeled pyrimidine and purine have been developed, they were used as probes for imaging herpes virus type one thymidine kinase (HSV1-tk) expression and other reporter genes. For example, pyrimidine nucleoside[41] and other ^{18}F-labeled acycloguanosine analogs[42–46] have
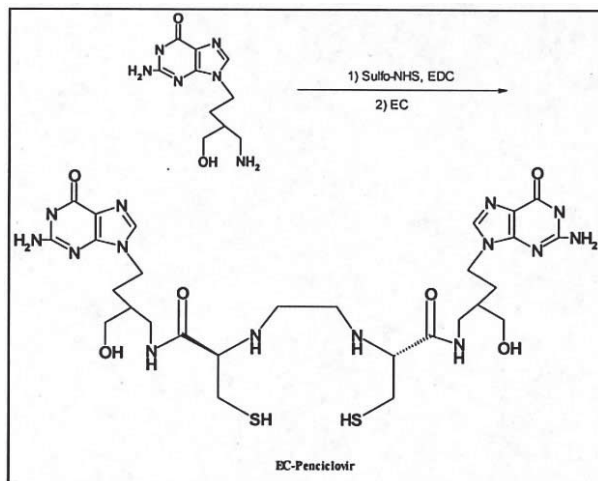
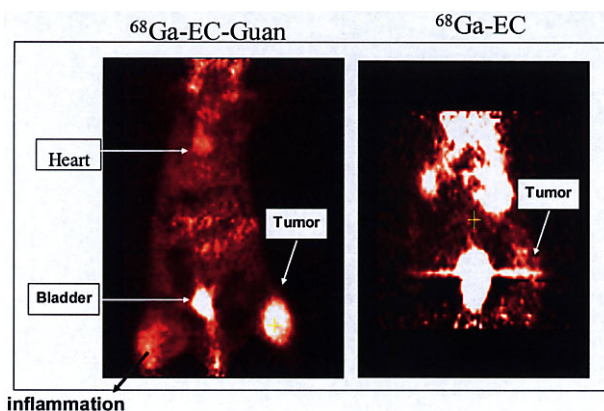**Fig. 2** Synthesis of EC-Guanine.

Fig. 3 Breast tumor (*right leg*) and inflammation (*left leg*, by turpentine, i.m.) bearing rats were administered with ^{68}Ga-EC-Guanine and ^{68}Ga-EC (control) (500 μCi /rat, i.v.). microPET of ^{68}Ga-EC-Guanine showed that tumor has much more uptake than inflammation at 1 hr post-injection.

Fig. 4 Structure of EC-metronidazole.

been developed as reporter substrates for imaging wild-type and mutant HSV1-tk expression. The difficulty with these probes is that HSV1-tk enzyme expression depends on HSV1-tk gene transduction with adenoviral vectors. The level of HSV1-tk enzyme expression is likely to be altered in different transduced cells and tissues; thus, the application of HSV1-tk probe is limited.

To overcome HSV1-tk enzyme expression, it would be desirable to develop a novel tracer to assess the efficacy of tumor therapy by measuring proliferative activity. Synthesis and biological activity of labeled thymidine or uridine, which were incorporated into DNA/RNA, have been reported.[47–49] However, either the complex chemistry, shorter half-life of radioisotope, or stability of the agent limited their practical use. We previously have reported that ^{18}F-labeled adenosine, a purine analogue, could measure proliferative activity by PET.[50] Other pyrimidine and purine nucleosides/nucleotides which were
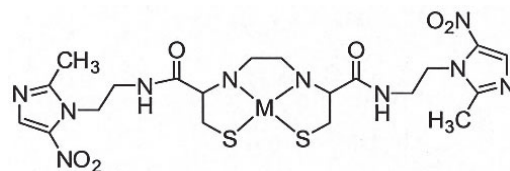
incorporated into DNA/RNA have been reported.[51–55] For instance, 3′-deoxy-3′-^{18}F-fluorothymidine (^{18}F-FLT) is a new tracer which images cellular proliferation by entering the salvage pathway of DNA synthesis. However, the DNA incorporation rate of FLT is low and chemistry is complex.[51,52] In order to enhance biological activity and increase chemical or metabolic stability, fluorine substitution at the C2′ position of the sugar moiety (arabino configuration) has been widely investigated in drug research.[53–56] Again, the chemistry is complex and the yield is low. To continuously explore other purine-based analogues using chelation radiochemistry, we then synthesized a guanine analogue using EC as a chelator. ^{99m}Tc- and ^{68}Ga-ethylenedicysteine-guanine (EC-Guan) were formulated for evaluation of cell proliferation. The synthetic scheme is shown in Figure 2. ^{68}Ga-EC-Guan was able to differentiate inflammation versus tumors (Fig. 3). *In vitro* cell confluence, cell cycle analysis, cellular uptake and *in vivo* imaging studies[57] suggest that ^{99m}Tc- and ^{68}Ga-EC-Guan may be useful as tumor proliferation imaging agents.

Assessment of angiogenesis

Angiogenesis, the proliferation of endothelial and smooth muscle cells to form new blood vessels, is an essential component of the metastatic pathway. These vessels provide the principal route by which tumor cells exit the primary tumor site and enter the circulation. For many tumors, the vascular density can provide a prognostic indicator of metastatic potential or survival, with highly vascularized tumors having a higher incidence of metastasis than poorly vascularized tumors.[58,59] There are four types of antiangiogenic therapy agents.[60–63] They are (1) antibodies, such as anti-integrins (Vitaxin), anti-EGFR (C225), anti-VEGF monoclonal antibody, anti-endoglin glycoprotein (anti-TGFβ); (2) protein fragments, such as plasminogen and collagen (endostatin); (3) modulation of FGF (interferons), and (4) synthetic small molecules, such as protease inhibitors, urokinase inhibitors, cyclooxygenase inhibitors and tyrosine kinase inhibitors. These new anti-angiogenic agents represent some of the more promising new approaches to anticancer therapy.

Though several agents were labeled with EC, the target assessment is not the same. Thus, labeled EC was used as a control for each agent itself comparison. ^{99m}Tc-EC-endostatin was synthesized and studied for its potential as
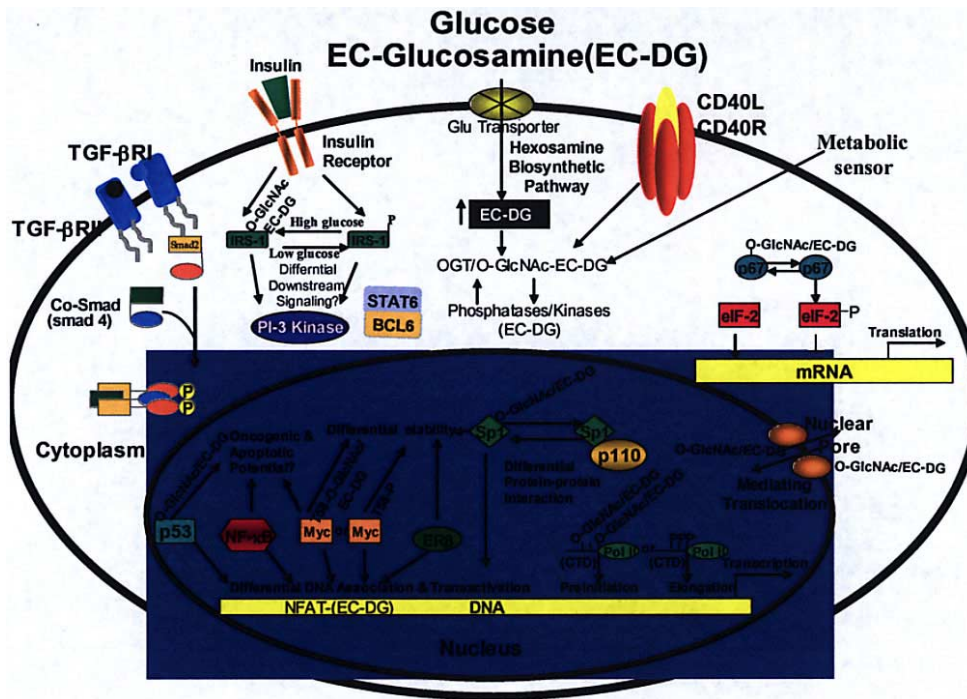
Fig. 5 The proposed mechanism of EC-DG suggests that EC-DG is phosphorylated and followed by *S-S*-linkage with protein and translocates to cell nuclei.
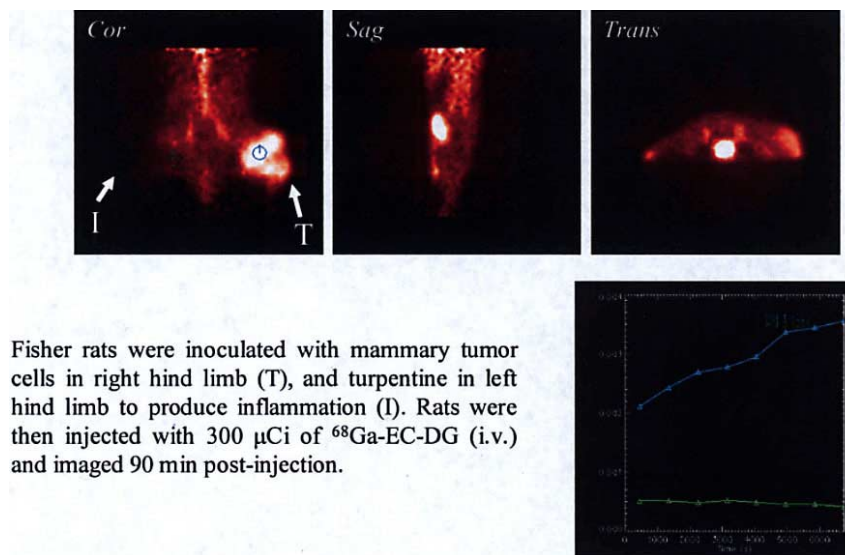
μPET Images of ^{18}F-FDG

Mammary tumor-bearing rats were injected with 300 μCi of ^{18}F-FDG (i.v.) and imaged 45 min post-injection.

Fig. 6 Breast tumor (*right leg*) and inflammation (*left leg*, by turpentine, i.m.) bearing rats were administered with ^{18}F-FDG (500 μCi /rat, i.v.). microPET of ^{18}F-FDG showed that tumor has much more uptake than inflammation at 45 min post-injection. T: tumor; I: Inflammation

a noninvasive imaging technique for the evaluation and measurement of tumor response to anti-angiogenic therapy. *In vitro* cell viability and TUNEL assays indicated no marked difference between EC-endostatin and endostatin. Cellular uptake assay suggests that endostatin binds to an endostatin receptor. Biodistribution of ^{99m}Tc-EC-endostatin in tumor-bearing rats showed increased tumor-to-tissue count density ratios as a function of time. Tumor uptake (%ID/g) of ^{99m}Tc-EC-endostatin was 0.2–0.5. Planar images confirmed that the tumors could be visualized clearly with ^{99m}Tc-EC-endostatin. The optimal time for imaging using radiolabeled endostatin was 2 hrs. ^{99m}Tc-EC-endostatin could also be used to assess treatment response. There was a correlation between tumor uptake and angiogenic target expression. Our results indicate that it may be feasible to use ^{99m}Tc-EC-endostatin

Fig. 7 Breast tumor (*right leg*) and inflammation (*left leg*, by turpentine, i.m.) bearing rats were administered with ^{68}Ga-EC-DG (500 μCi /rat, i.v.). microPET of ^{68}Ga-EC-DG showed that tumor has high uptake whereas inflammation showed poor uptake at dynamic acquisition up to 90 min post-administration. T: tumor; I: Inflammation
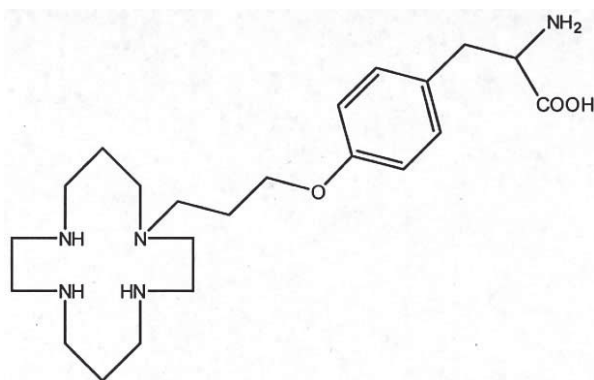

Fig. 8 Synthesis of cyclam-tyrosine.

to assess the efficiency of anti-angiogenesis therapy.[13]

Cyclooxygenase-2 (COX-2) plays an important role in angiogenesis and cancer progression.[64] Since many tumor cells exhibit COX-2 expression, functional imaging of COX-2 expression using Celebrex (CBX, a COX-2 inhibitor) may provide not only a non-invasive, reproducible, quantifiable alternative to biopsies, but would also greatly complement pharmacokinetic studies by correlating clinical responses with biological effects. Moreover, molecular endpoints of anti-COX-2 therapy could also be assessed effectively. We have developed ^{99m}Tc-EC-Celecoxib (EC-CBX) for measurement of COX-2 expression in tumor bearing animal models. We conclude that ^{99m}Tc-EC-CBX may be useful to assess tumor COX-2

expression.[19] This may be useful in the future for selecting patients for treatment with anti-COX-2 agents.

Epidermal Growth Factor Receptor (EGFR) plays an important role in cell division and cancer progression, as well as angiogenesis and metastasis. Since many tumor cells express EGFR on their surface, functional imaging of EGFR provides not only a non-invasive, reproducible, quantifiable alternative to biopsies, but it also greatly complements pharmacokinetic studies by correlating clinical responses with biological effects.[65,66] Moreover, molecular endpoints of anti-EGFR therapy could be assessed effectively. C225 is a chimeric monoclonal antibody that targets the human extracellular EGFR and inhibits the growth of EGFR-expressing tumor cells. Also, it has been demonstrated that C225, in combination with chemotherapeutic drugs or radiotherapy, is effective in eradicating well-established tumors in nude mice. We have developed ^{99m}Tc-EC-C225 and imaged EGFR-positive tumor bearing animal models. The preliminary feasibility of imaging patients with head and neck carcinomas was also evaluated. Our findings indicate that ^{99m}Tc-EC-C225 is useful to assess tumor EGFR expression.[14] This may be useful in the future for selecting patients for treatment with C225.

Assessment of tumor hypoxia

It is well established in experimental and clinical studies that most tumors have a considerable proportion of hypoxic cells. Hypoxic tumors are known to be resistant to traditional radio- and chemotherapy, which results in
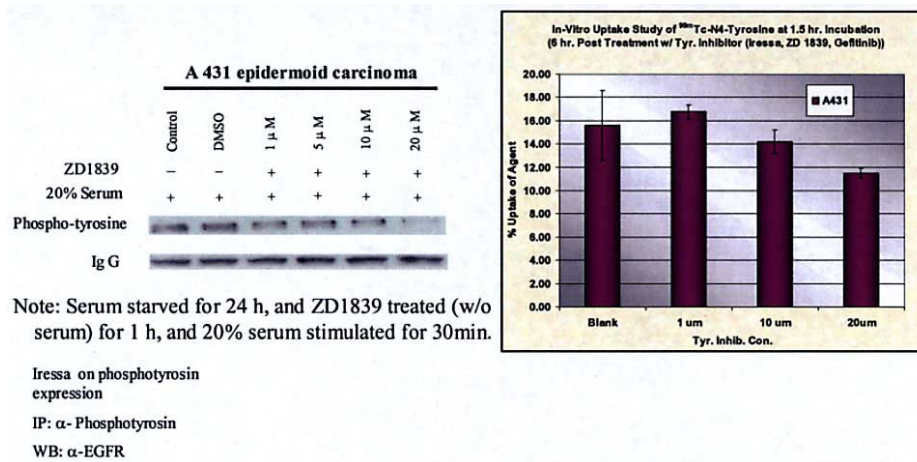
Fig. 9 Western blot analysis showed that the expression of tyrosinase in A431 cells could be blocked by Iressa at higher concentrations. *In vitro* cellular uptake of ^{99m}Tc-cyclam-tyrosine showed decreased uptake in the cells treated with higher concentration of Iressa. Cellular uptake studies correlate well with Western blot assays.
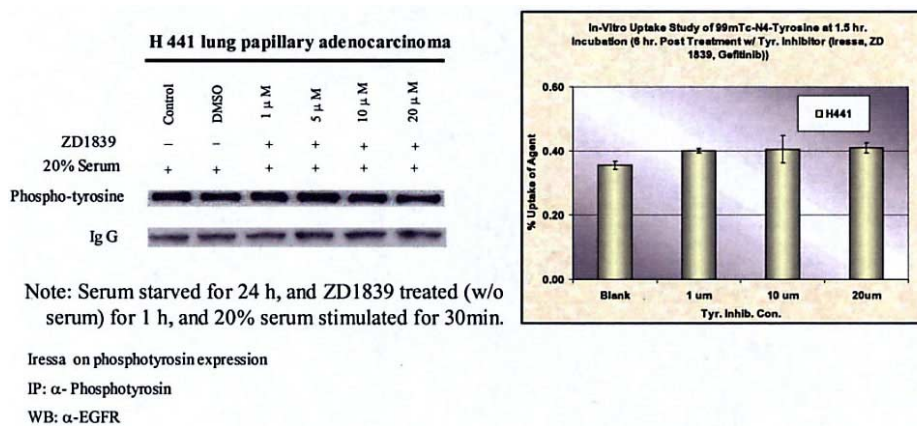

Fig. 10 Western blot analysis showed that the expression of tyrosinase in H441 cells could not be blocked by Iressa at higher concentrations. *In vitro* cellular uptake of ^{99m}Tc-cyclam-tyrosine showed no marked uptake changes in the cells treated with higher concentration of Iressa. Cellular uptake studies correlate well with Western blot assays.

higher local recurrence rates. Hypoxia also induces angiogenesis and adds to the invasive and metastatic potential of cancer cells and further compromises the therapeutic outcome. Efforts have been made to develop relevant and efficient non-invasive methods to assess the presence and extent of tumor hypoxia in patients but have met little success. The ability to quantify tissue hypoxia will allow the physicians to select patients for additional or alternative treatment regimens that would circumvent the ominous impact of hypoxia.[17] Metronidazole (MN), a 5-nitroimidazole analogue, was shown to sensitize only anoxic cells in a dose dependent manner, a maximum enhancement ratio of 1.9 being obtained (2.5 for MISO).[67] EC-MN was then synthesized and the structure is shown in Figure 4. Clinical studies showed that ^{99m}Tc-EC-MN was able to differentiate hypoxic regions in stroke pa-

tients.[17] The findings indicate that EC-MN is a hypoxic marker.

Assessment of metabolic imaging

There is a structural similarity between FDG and glucosamine. For instance, both agents have the same configuration. FDG and glucosamine have fluorine and amino group at the position-2 of the sugar. Similarly to FDG, cellular uptake of glucosamine is via the glucose transporter process.[15] However, the regulatory products of glucosamine-6-phosphate mediate insulin activation, downstream signaling and translocation, which upregulate mRNA expression and tumor growth.

Our previous work demonstrated that tumor uptake of ^{99m}Tc-EC-DG is via a glucose-mediated process.[15,68] One reason may be that the molecule (EC-DG) has mul-

tiple key structural position(s), such as positions 2 and 6 for D-glucosamine and the two COO- arms and two thiol (SH) locations for EC. During synthesis, the molecule changes via a peptide-linkage between the 2 position of the sugar with EC and occurs at both carboxy groups of EC. EC forms a peptide bond linkage with 2 thiols which can react with glycoproteins in the lumen of the cell membrane, such as O-linked N-acetylglucosamine.[69–72] It is likely that SH bonds of EC-DG bind to cytosolic and transmembrane enzymes (Beta-N-acetylglucosaminidase and O-GlcNAc transferase) or membrane associated proteins (O-linked N-acetylglucosamine) which form (EC-DG) S-S (protein) linkages and support the translocation of EC-DG into the cell nucleus. It is known that glucosamine is phosphorylated at positions 1 and 6 and binds with uridine diphospho-N-acetylglucosamine to form O-linked N-acetylglucosamine at those same positions, which involves interaction between nuclear and cytosolic proteins. Recent studies demonstrate a role for O-GlcNAcylation in processes as diverse as transcription in the nucleus and signaling in the cytoplasm, suggesting that O-GlcNAc has both protein and site-specific influences on biochemistry and metabolism throughout the cell.[69,70] We believe that it is this mechanism that is occurring which makes EC-DG so unique in its ability to be internalized by the cell. The possible mechanism is shown in Figure 5.

The animal imaging studies showed that ^{68}Ga-EC-DG could differentiate inflammation vs. tumor better than FDG (Figs. 6, 7) and ^{68}Ga-EC-DG may be used for evaluation of the therapeutic tumor response.

Assessment of tyrosine kinase activity
Tyrosine kinase inhibitors (Iressa, Tarceva) have shown efficacy against tumor growth. We have synthesized cyclam-tyrosine. The structure is shown in Figure 8. There was a good biologic correlation between Western blot analysis and ^{99m}Tc-cyclam-tyrosine cellular uptake (Figs. 9, 10). The tumors with high expression of tyrosine kinases correlate well with cell culture data. The high expression of tyrosine activity could be blocked by Iressa (Fig. 9). The findings indicate that ^{99m}Tc-cyclam-tyrosine may be useful in selecting patients who may respond to tyrosinase therapy.

CONCLUSION

Noninvasive imaging assessment of tumor cell proliferation could be helpful in the evaluation of tumor growth potential, the degree of malignancy, and could provide an early assessment of treatment response prior to changes in tumor size determined by computed tomography (CT), magnetic resonance imaging (MRI), or ultrasonography. Understanding of tumor proliferative activity, in turn, could aid in the selection of optimal therapy by estimating patient prognosis and selecting the proper management.

Aiming to develop new radiolabeled ligands for metabolic imaging of tumors, a series of new ligands have been developed for PET and SPECT imaging of neoplasms. For apoptosis assessment, radiolabeled EC-annexin V showed the potential to predict early treatment response. For DNA/RNA markers, EC-Guan showed promising results in differentiating inflammation versus tumor. For angiogenesis imaging, EC-endostatin, EC-CBX and EC-C225 are adequate to assess specific targets. For tumor hypoxia imaging, a classic nitroimidazole agent such as metronidazole is useful to monitor treatment response and may have potential in drug resistance or radioresistance imaging. Our metabolic imaging agent, radiolabeled EC-DG could assess tumor growth. Radiolabeled tyrosine could monitor tyrosine kinase activity. All of these functional ligands should provide information for prediction or monitoring of the treatment response of tumors. Thus, they may improve the diagnosis, planning and monitoring of cancer treatment.

REFERENCES

1. Kubota K, Ishiwata K, Kubota R, et al. Tracer feasibility for monitoring tumor radiotherapy: A quadruple tracer study with fluorine-18-fluorodeoxyglucose or fluorine-18-fluorodeoxyuridine, L-[methy1-^{14}C]methionine, [6-^{3}H]thymidine, and gallium-67. *J Nucl Med* 1991; 32: 2118–2123.
2. Tjuvajev J, Muraki A, Ginos J, et al. Iododeoxyuridine uptake and retention as a measure of tumor growth. *J Nucl Med* 1993; 34: 1152–1162.
3. Strauss LG, Conti PS. The application of PET in clinical oncology. *J Nucl Med* 1991; 32: 623–648.
4. Ohtsuki K, Akashi K, Aoka Y, et al. Technetium-99m HYNIC-annexin V: a potential radiopharmaceutical for the *in-vivo* detection of apoptosis. *Eur J Nucl Med* 1999; 26 (10): 1251–1258.
5. Vriens PW, Blankenberg FG, Stoot JH, et al. The use of technetium ^{99m}Tc annexin V for *in vivo* imaging of apoptosis during cardiac allograft rejection. *J Thorac Cardiovasc Surg* 1998; 116: 844–853.
6. Van Nerom CG, Bormans GM, De Roo MJ, et al. First experience in healthy volunteers with technetium-99m L,L-ethylenedicysteine, a new renal imaging agent. *Eur J Nucl Med* 1993; 20: 738–746.
7. Canet EP, Casali C, Desenfant A, et al. Kinetic characterization of CMD-A2-Gd-DOTA as an intravascular contrast agent for myocardial perfusion measurement with MRI. *Magn Reson Med* 2000; 43 (3): 403–409.
8. Laissy JP, Faraggi M, Lebtahi R, et al. Functional evaluation of normal and ischemic kidney by means of gadolinium-DOTA enhanced TurboFLASH MR imaging: a preliminary comparison with ^{99m}Tc-MAG3 dynamic scintigraphy. *Magn Reson Imaging* 1994; 12 (3): 413–419.
9. Kao CH, ChangLai SP, Chieng PU, et al. Technetium-99m methoxyisobutylisonitrile chest imaging of small cell lung carcinoma: relation to patient prognosis and chemotherapy response—a preliminary report. *Cancer* 1998; 83: 64–68.
10. Wu HC, Chang CH, Lai MM, et al. Using Tc-99m DMSA

renal cortex scan to detect renal damage in women with type 2 diabetes. *J Diabetes Complications* 2003; 17: 297–300.

11. Zareneyrizi F, Yang DJ, Oh CS, et al. Synthesis of ^{99m}Tc-ethylenedicysteine-colchicine for evaluation of antiangiogenic effect. *Anticancer Drugs* 1999: 10: 685–692.

12. Yang DJ, Azhdarinia A, Wu P, et al. *In vivo* and *in vitro* measurement of apoptosis in breast cancer cells using ^{99m}Tc-EC-annexin V. *Cancer Biother Radiopharm* 2001: 16: 73–83.

13. Yang DJ, Kim KD, Schechter NR, et al. Assessment of antiangiogenic effect using ^{99m}Tc-EC-endostatin. *Cancer Biother Radiopharm* 2002: 17: 233–245.

14. Schechter NR, Yang DJ, Azhdarinia A, et al. Assessment of epidermal growth factor receptor with ^{99m}Tc-ethylenedicysteine-C225 monoclonal antibody. *Anticancer Drugs* 2003: 14: 49–56.

15. Yang DJ, Kim CG, Schechter NR, et al. Imaging with ^{99m}Tc ECDG targeted at the multifunctional glucose transport system: feasibility study with rodents. *Radiology* 2003: 226: 465–473.

16. Ilgan S, Yang DJ, Higuchi T, et al. ^{99m}Tc-Ethylenedicysteine-Folate: A new tumor imaging agent. Synthesis, labeling and evaluation in animals. *Cancer Biotherapy and Radiopharm* 1998: 13: 427–435.

17. Song HC, Bom HS, Cho KH, et al. Prognostication of recovery in patients with acute ischemic stroke using brain SPECT with ^{99m}Tc-metronidazole. *Stroke* 2003: 34: 982–986.

18. Yang DJ, Bryant J, Chang JY, et al. Assessment of COX-2 expression with ^{99m}Tc-labeled celebrex. *Anti-Cancer Drugs* 2004: 15: 255–263.

19. Zheng YY, Saluja S, Yap GP, et al. Gallium and Indium Complexes of Bis(amino thiol) (N(2)S(2)) Ligands. *Inorg Chem* 1996: 35: 6656–6666.

20. Anderson CJ, John CS, Li YJ, et al. *N,N′*-ethylene-di-L-cysteine (EC) complexes of Ga(III) and In(III): molecular modeling, thermodynamic stability and *in vivo* studies. *Nucl Med Biol* 1995: 22: 165–173.

21. Sun Y, Anderson CJ, Pajeau TS, et al. Indium (III) and gallium (III) complexes of bis(aminoethanethiol) ligands with different denticities: stabilities, molecular modeling, and *in vivo* behavior. *J Med Chem* 1996: 39: 458–470.

22. Sanchez-Crespo A, Andreo P, Larsson SA. Positron flight in human tissues and its influence on PET image spatial resolution. *Eur J Nucl Med Mol Imaging* 2004; 31: 44–51.

23. Grove NB, Martin MJ. Log-f tables for beta decay. *Nucl Data Tables* 1971; 205.

24. Motekaitis RJ. The Gallium (III) and Indium (III) Complexes of Tris (2-mercapto benzyl) amine and Tris (2-hydroxylbenzyl) amine. *Inorg Chem* 1998; 37: 5902–5911.

25. Reichert DE, Hancock RD, Welch MJ. Molecular Mechanics Investigation of Gadolinium(III) Complexes. *Inorg Chem* 1996; 35: 7013–7020.

26. Mathias CJ, Lewis MR, Reichert DE, et al. Preparation of [66]Ga- and ^{68}Ga-labeled Ga(III)-deferoxamine-folate as potential folate-receptor-targeted PET radiopharmaceuticals. *Nucl Med Biol* 2003; 30: 725–731.

27. Denmeade SR, Isaacs JT. Programmed cell death (apoptosis) and cancer chemotherapy: Cancer Control. *Cancer Control* 1996; 3 (4): 1996.

28. Garzetti GG, Ciavattini A, Provincial M, et al. Expression of p53 and apoptosis of tumor cells in locally advanced cervical carcinoma after cisplatin based neoadjuvant chemotherapy. *Anticancer Res* 1996; 16: 3229–3224.

29. Wheeler JA, Stephens LC, Tornos C, et al. ASTRO research fellowship: apoptosis as a predictor of tumor response to radiation in stage IB cervical carcinoma. *Int J Rad Oncol Biol Phys* 1995; 32 (5): 1487–1493.

30. Meyn RE, Stephens LC, Hunter NR, et al. Induction of apoptosis in murine tumors by cyclophosphamide. *Cancer Chem Pharm* 1994; 33: 410–414.

31. Meyn RE, Stephens LC, Hunter NR, et al. Kinetics of cisplatin-induced apoptosis in murine mammary and ovarian adenocarcinomas. *Int J Cancer* 1995; 60: 725–729.

32. Meyn RE, Stephens LC, Hunter NR, et al. Apoptosis in murine tumors treated with chemotherapy agents. *Anti-Cancer Drugs* 1995; 6: 443–450.

33. Meyn RE, Stephens LC, Mason KA, et al. Radiation-induced apoptosis in normal and pre-neoplastic mammary glands *in vivo*: Significance of gland differentiation and p53 status. *Int J Cancer* 1996; 65: 466–472.

34. Buchholz TA, Davis DW, McConkey DJ, et al. Chemotherapy-induced apoptosis and Bcl-2 levels correlate with breast cancer response to chemotherapy. *Cancer J* 2003; 9 (1): 33–41.

35. Symmans WF, Volm MD, Shapiro RL, et al. Paclitaxel-induced apoptosis and mitotic arrest assessed by serial fine-needle aspiration: implications for early prediction of breast cancer response to neoadjuvant treatment. *Clin Cancer Res* 2000; 6 (12): 4610–4617.

36. Ueno T, Toi M, Bivén K, et al. Measurement of an apoptosis product in the sera of breast cancer patients. *Eur J Cancer* 2003; 39: 769–774.

37. Okada J, Yoshihawa K, Itami M, et al. Positron emission tomography using fluorine-18-fluorodeoxyglucose in malignant lymphoma: A comparison with proliferative activity. *J Nucl Med* 1992; 33: 325–329.

38. Higashi K, Clavo AC, Wahl RL. Does FDG uptake measure proliferative activity of human cancer cells? *In vitro* comparision with DNA flow cytometry and tritiated thymidine uptake. *J Nucl Med* 1992; 34: 414–419.

39. McConathy J, Martarello L, Malveaux EJ, et al. Synthesis and evaluation of 2-amino-4-[(18)F]fluoro-2-methyl-butanoic acid (FAMB): relationship of amino acid transport to tumor imaging properties of branched fluorinated amino acids. *Nucl Med Biol* 2003; 30: 477–490.

40. Jager PL, Plaat BE, de Vries EG, et al. Imaging of soft-tissue tumors using L-3-[iodine-123]iodo-alpha-methyl-tyrosine single photon emission computed tomography: comparison with proliferative and mitotic activity, cellularity, and vascularity. *Clin Cancer Res* 2000; 6: 2252–2259.

41. Tjuvajev JG, Doubrovin M, Akhurst T, et al. Comparison of radiolabeled nucleoside probes (FIAU, FHBG, and FHPG) for PET imaging of HSV1-tk gene expression. *J Nucl Med* 2002; 43: 1072–1083.

42. Namavari M, Barrio JR, Toyokuni T, et al. Synthesis of 8-[^{18}F]fluoroguanine derivatives: *in vivo* probes for imaging gene expression with positron emission tomography. *Nucl Med Biol* 2000; 27: 157–162.

43. Gambhir SS, Bauer E, Black ME, et al. A mutant herpes simplex virus type 1 thymidine kinase reporter gene shows improved sensitivity for imaging reporter gene expression

with positron emission tomography. *Proc Natl Acad Sci USA* 2000; 97: 2785–2790.

44. Iyer M, Barrio JR, Namavari M, et al. 8-[^{18}F]Fluoro-penciclovir: an improved reporter probe for imaging HSV1-tk reporter gene expression *in vivo* using PET. *J Nucl Med* 2001; 42: 96–105.

45. Alauddin MM, Shahinian A, Kundu RK, et al. Evaluation of 9-[(3-^{18}F-fluoro-1-hydroxy-2-propoxy)methyl]guanine ([^{18}F]-FHPG) *in vitro* and *in vivo* as a probe for PET imaging of gene incorporation and expression in tumors. *Nucl Med Biol* 1999; 26: 371–376.

46. Yaghoubi S, Barrio JR, Dahlbom M, et al. Human pharmacokinetic and dosimetry studies of [^{18}F]FHBG: a reporter probe for imaging herpes simplex virus type-1 thymidine kinase reporter gene expression. *J Nucl Med* 2001; 42: 1225–1234.

47. Goethals P, Eijkeren MV, Lodewyck W, et al. Measurement of [methyl-carbon-11]thymidine and its metabolites in head and neck tumors. *J Nucl Med* 1995; 36: 880–882.

48. Tjuvajev J, Macapinlac HA, Daghighian F, et al. Imaging of brain tumor proliferative activity with iodine-131-iodo-deoxyuridine. *J Nucl Med* 1994; 35: 1407–1417.

49. Abe Y, Fukuda H, Ishiwata K, et al. Studies on ^{18}F-Labeled Pyrimidines Tumor Uptakes of ^{18}F-5-Fluorouracil, ^{18}F-5-Fluorouridine, and ^{18}F-5-Fluorodeoxyuridine in Animals. *Eur J Nucl Med* 1983; 8: 258–261.

50. Kim CG, Yang DJ, Kim EE, et al. Assessment of tumor cell proliferation using [^{18}F]fluorodeoxyadenosine and [^{18}F]fluoroethyluracil. *J Pharm Sci* 1996; 85: 339–344.

51. Buck AK, Halter G, Schirrmeister H, et al. Imaging Proliferation in Lung Tumors with PET: ^{18}F-FLT Versus ^{18}F-FDG. *J Nucl Med* 2003; 44: 1426–1431.

52. Francis DL, Visvikis D, Costa DC, et al. Potential impact of [^{18}F]3′-deoxy-3′-fluorothymidine versus [^{18}F]fluoro-2-deoxy-D-glucose in positron emission tomography for colorectal cancer. *Eur J Nucl Med Mol Imaging* 2003; 30: 988–994.

53. Marquez VE, Tseng CKH, Mitsuya H, et al. Acid-stable 2′-fluoro purine dideoxynucleosides as active agents against HIV. *J Med Chem* 1990; 33: 978–985.

54. Wright JA, Taylor NF, Fox JJ. Nucleosides. LX. Fluorocarbohydrates. synthesis of 2-deoxy-2-fluoro-D-arabinose and 9-(2-deoxy-2-fluoro-α- and -β-D-arabino-furanosyl)-adenines. *J Org Chem* 1969; 34: 2632–263?.

55. Uesugi S, Kaneyasu T, Ikehara M. Synthesis and properties of ApU Analogues containing 2′-halo-2′-deoxyadenosine. Effect of 2′ substituents on oligonucleotide conformation. *Biochemistry* 1982; 21: 5870–5877.

56. Ikehara M, Miki H. Studies of nucleosides and nucleotides. Cyclonucleosides. Synthesis and properties of 2′-halogeno-2′-deoxyadenosines. *Chem Pharm Bul* 1978; 26: 2449–2453.

57. Chao KC, Yang DJ, Yang T, Azhdarinia A. Assessment of DNA/RNA proliferation using radiolabeled guanine analogues by PET and SPECT. *Molecular Imaging and Biology* 2004; 6 (2): 107. (abstract)

58. Bertolini F, Paolucci M, Peccatori F, et al. Angiogenic growth factors and endostatin in non-Hodgkin's lymphoma. *Br J Haematol* 1999; 106: 504–509.

59. Smith BD, Smith GL, Carter D, et al. Prognostic significance of vascular endothelial growth factor protein levels in oral and oropharyngeal squamous cell carcinoma. *J Clin Oncol* 2000; 18: 2046–2052.

60. Feltis BA, Sahar DA, Kim AS, Saltzman DA, Leonard AS, Sielaff TD. Cyclooxygenase-2 inhibition augments the hepatic antitumor effect of oral salmonella typhimurium in a model of mouse metastatic colon cancer. *Dis Colon Rectum* 2002; 45: 1023–1028.

61. Decatris M, Santhanam S, O'Byrne K. Potential of Interferon-alpha in Solid Tumours: Part 1. *BioDrugs* 2002; 16: 261–281.

62. Baselga J, Albanell J. Targeting epidermal growth factor receptor in lung cancer. *Curr Oncol Rep* 2002; 4: 317–324.

63. Herbst RS, Shin DM. Monoclonal antibodies to target epidermal growth factor receptor-positive tumors: a new paradigm for cancer therapy. *Cancer* 2002; 94: 1593–1611.

64. Alshafie GA, Abou-Issa HM, Seibert K, Harris RE. Chemotherapeutic evaluation of Celecoxib, a cyclooxygenase-2 inhibitor, in a rat mammary tumor model. *Oncol Rep* 2000; 7: 1377–1381.

65. Waxman ES, Herbst RS. The role of the epidermal growth factor receptor in the treatment of colorectal carcinoma. *Semin Oncol Nurs* 2002; 18: 20–29.

66. Ciardiello F, Tortora G. A novel approach in the treatment of cancer: targeting the epidermal growth factor receptor. *Clin Cancer Res* 2001; 7: 2958–2970.

67. Yang DJ, Ilgan, S, Higuchi T, et al. Noninvasive assessment of tumor hypoxia with ^{99m}Tc-labeled metronidazole. *Pharm Res* 1999; 16: 743–750.

68. Yang DJ, Yukihiro M, Oh C-S, et al. Assessment of Therapeutic Tumor Response Using ^{99m}Tc-Ethylenedicysteine-Glucosamine. *Cancer Biotherapy and Radiopharm* 2004; 19 (4): 444–458.

69. Marshall S, Bacote V, Traxinger RR. Discovery of a metabolic pathway mediating glucose-induced desensitization of the glucose transport system. *J Biol Chem* 1991; 266: 4706–4712.

70. Wells L, Gao Y, Mahoney JA, et al. Dynamic *O*-glycosylation of nuclear and cytosolic proteins: further characterization of the nucleocytoplasmic beta-*N*-acetylglucosaminidase, *O*-GlcNAcase, *J Biol Chem* 2002; 277: 1755–1761.

71. Pal S, Claffey KP, Cohen HT, Mukhopadhyay D. Activation of Sp1-mediated vascular permeability factor/vascular endothelial growth factor transcription requires specific interaction with protein kinase C zeta. *J Biol Chem* 1998; 273: 26277–26280.

72. Black AR, Black JD, Azizkhan-Clifford J. Sp1 and kruppel-like factor family of transcription factors in cell growth regulation and cancer. *J Cell Physiol* 2001; 188: 143–160.